

# Robo-GS: A Physics Consistent Spatial-Temporal Model for Robotic Arm with Hybrid Representation

Haozhe Lou<sup>1\*</sup>, Yurong Liu<sup>2\*</sup>, Yike Pan<sup>3\*</sup>, Yiran Geng<sup>4\*</sup>, Jianteng Chen<sup>5\*</sup>, Wenlong Ma<sup>6</sup>, Chenglong Li<sup>6</sup>, Lin Wang<sup>6</sup>, Hengzhen Feng<sup>6</sup>, Lu Shi<sup>9</sup>, Liyi Luo<sup>8</sup>, Yongliang Shi<sup>†7</sup>

**Abstract**— Real2Sim2Real plays a critical role in robotic arm control and reinforcement learning, yet bridging this gap remains a significant challenge due to the complex physical properties of robots and the objects they manipulate. Existing methods lack a comprehensive solution to accurately reconstruct real-world objects with spatial representations and their associated physics attributes.

We propose a Real2Sim pipeline with a hybrid representation model that integrates mesh geometry, 3D Gaussian kernels, and physics attributes to enhance the digital asset representation of robotic arms.

This hybrid representation is implemented through a Gaussian-Mesh-Pixel binding technique, which establishes an isomorphic mapping between mesh vertices and Gaussian models. This enables a fully differentiable rendering pipeline that can be optimized through numerical solvers, achieves high-fidelity rendering via Gaussian Splatting, and facilitates physically plausible simulation of the robotic arm’s interaction with its environment using mesh-based methods.

Given the digital assets, we propose a manipulable Real2Sim pipeline that standardizes coordinate systems and scales, ensuring the seamless integration of multiple components. In addition to reconstructing the robotic arm, the surrounding static background and objects can be holistically reconstructed, enabling seamless interactions between the robotic arm and its environment.

We also provide datasets covering various robotic manipulation tasks and robotic arm mesh reconstructions. These datasets include real-world motion captured in digital assets, ensuring precise representation of mass and friction, which are crucial for robotic manipulation. Our model achieves state-of-the-art results in realistic rendering and mesh reconstruction quality for robotic applications. The code, full presentation and datasets will be made publicly available at our website <https://robostudioapp.com/>

## I. INTRODUCTION

The Real2Sim2Real (R2S2R) paradigm is critical for advancing robotic learning, but it has yet to be fully realized due to significant challenges in spatial and color representation, as well as rendering quality, within current Real2Sim approaches [2]. These challenges hinder the effective transfer of learned policies from simulation to real-world

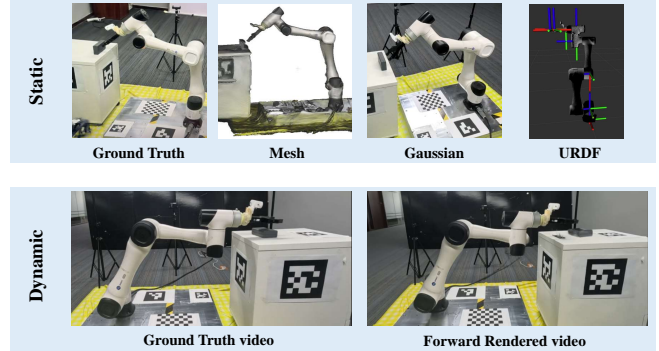


Fig. 1. The digital assets in our datasets include the extraction of the mesh based on monocular panoptic-labeled video, Gaussian Models[1], a kinematic and dynamically consistent URDF model, the dynamic ground truth video, and rendered video of policy implementation.

applications, compromising the reliability and performance of robotic systems trained in simulated environments.

In this paper, we target the holistic reconstruction of robotic arm operation scenes, which requires a manipulable robot model, the reconstruction of the background and objects, the incorporation of physical parameters such as mass and friction, and a realistic renderer. Our approach employs Unified Robot Description Format(URDF) [3], [4] as a spatial representation and integrates governing equations with physics parameters as the forward deformation mechanism. This combination enables accurate collision detection and consistent rendering across both simulation and Gaussian Splatting environments [5], [6].

Central to our method is a Gaussian-Mesh-Pixel binding, which establishes an isomorphic relationship between mesh vertices, Gaussian kernels [1], and image pixels. Each Gaussian is assigned a semantic label and a corresponding ID, enabling the precise application of transformation matrices governed by the URDF. This ensures a seamless transfer of trajectories between real-world video, simulation results, and rendered images. The advantages of this binding include end-to-end differentiable gradient passing between each representation, superior collision detection through our state-of-the-art mesh reconstruction, and high rendering quality.

Our system ensures consistent rendering between simulation and reality, allowing learned policies to be effectively deployed in real-world scenarios. Additionally, it supports editing within the Isaac Sim (Gym) [6], [7] simulation

\*Equal contribution, †Corresponding author

<sup>1</sup>University of Southern California

<sup>2</sup>National University of Singapore

<sup>3</sup>University of Michigan, Ann Arbor

<sup>4</sup>Peking University

<sup>5</sup>Hong Kong University of Science and Technology

<sup>6</sup>Beijing Institute of Technology

<sup>7</sup>Tsinghua University

<sup>8</sup>Xiaomi Robotics Lab

<sup>9</sup>AIR, Tsinghua University

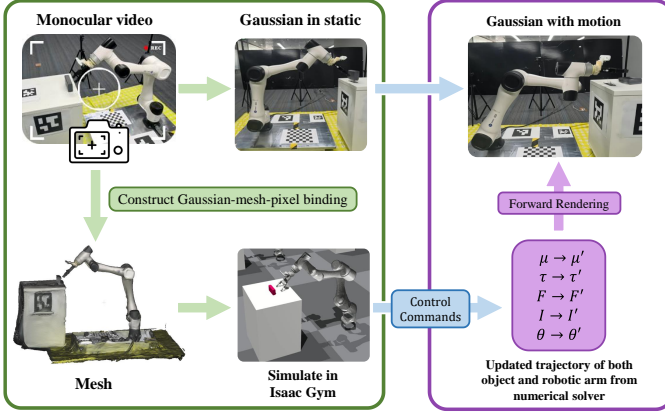


Fig. 2. Our method generates the Mesh and Gaussian from monocular video; and produce URDF of object, robotic arm and background from mesh; the URDF can generate trajectory to Gaussian through our Gaussian-mesh-pixel binding; Then we will use our renderer to perform forward deformation.

backend, enabling novel-pose and novel-policy adjustments. Optimized for robotic arms in CR [8] and UR [9] product sequences, our method is versatile enough to generalize to other robotic arm models. Our method achieves state-of-the-art performance in video-based mesh reconstruction and dynamic rendering compared to current methods [10].

Furthermore, we propose a new format for digital assets, represented by a combination of mesh, Gaussian Splatting, and real-world motion, as shown in 1 [11]. This approach surpasses traditional textured mesh and material attributes by integrating critical physics parameters, such as mass and friction, extracted from real-world motion videos [12].

## II. RELATED WORK

The Real2Sim2Real paradigm, essential for bridging the gap between physical and simulated environments, requires rendering, asset extraction, and control.

*Rendering:* One of the most direct methods involves utilizing 3D reconstruction techniques such as Gaussian Splatting and Neural Radiance Fields (NeRF) [1], [13], [14], [15], [16]. These techniques have revolutionized the creation of high-fidelity digital twins of real-world objects, essential for accurate simulations.

Recent advancements in robotic simulation have leveraged transformation matrices and Linear Blend Skinning (LBS) [17] control modes for enhanced fidelity. However, the geometric consistency of robotic arms often suffers due to the reliance on rigid mesh motions. The work presented in SC-GS [18] addresses this limitation by minimizing unnecessary errors through sparse control points, although it falls short in accurately simulating robotic arm motions. Furthermore, works such as those detailed in [19] [10] and [20] employ NeRFs and Gaussian splatting for reconstructing robotic operation scenes and implementing simulations. Additionally, the exploration of Gaussian-based, highly deformable object reconstruction, as seen in MD-Splatting [21], utilizes neural radiance fields and particle-based representations for robotic simulation and grasping tasks. However, these meth-

ods often fall short of enabling high-fidelity rendering [22]. Thus, for realistic rendering, traditional MLP-based deformation fields [18], [23] are replaced with numerical ODE solvers [24], [25] to enhance the quality of 4D Gaussian splatting in our method.

*Asset production:* In the realm of mesh reconstruction and simulation integration, NeRFmeshing [26], SUGAR [27], [28], [29] represent significant advancements. NeRFmeshing uses NeRFs for mesh reconstruction, while SUGAR employs Gaussian splatting for mesh extraction, yielding impressive results. However, the sparsity and complexity of robotic arm structures often result in non-smooth reconstructions due to challenges in normal estimation. The 2DGS method [30] successfully addresses the issue of non-smooth surfaces by introducing a planar-like 2D Gaussian Splatting representation. The quality of meshes generated by 2DGS proves sufficient for robotic simulation after several cleaning and matching techniques.

*Control:* The control of robotic arms within the Real2Sim2Real paradigm typically employs pose-based control, where the trajectory of the end-effector pose [31] is transferred between real-world and simulation policies. This method utilizes inverse kinematics to derive Pre-joint control information [32]. Current Real2Sim2Real control policies include diffusion-based models [33] and trajectory-to-video generation methods like IRASim [34], which use generative methods driven by trajectory for simulation and representation. However, these methods are limited to fully represent 3D and 4D real-world scenarios. [35], [36], [37], [38], [39], [40].

Classical control of robotic arms connects each linkage with predefined joints, using angles to control the path [41], [42], [43]. In a Gaussian setting, there is no definition of linkage, and each Gaussian is treated as an independent element, leading to motion inconsistencies. Our method addresses this issue through isomorphism Mesh-Gaussian binding.

Recent developments include a signed distance field-based approach for robotic arm morphology [44]. This method utilizes joint angles as input, with a neural decoder guiding the deformation field. However, it lacks explicit compatibility with the MOVEIT path-based control pipeline [45] and current reinforcement training toolkit [41]. SimPLE [46] uses tactile sensors and a depth camera along with a pre-built CAD model to implement grasp and robotic arm tasks. The UMI on Legs shows the potential of simulation-based manipulation tasks but the reconstruction of scenes and objects is still missing [47].

In contrast, Physically embodied gaussian splatting [48] employ Gaussian distributions and particles derived from Pre-built meshes to generate movement, tested on simulated data. Our approach advances this by utilizing meshes extracted from video data for a more accurate representation, coupled with real-world scenario data collection.

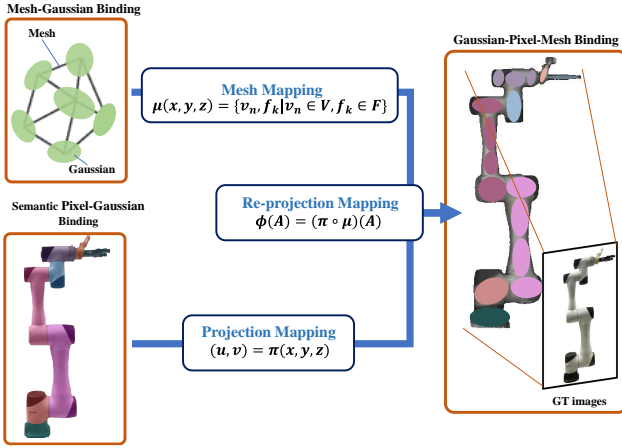


Fig. 3. Gaussian-Mesh-Pixel binding.

### III. METHOD

#### A. Representation

Our digital asset is represented by the mesh, Gaussian Splatting, and real-world motion. In the traditional production of digital asset, it focuses on the textured mesh and materials attribute. However, we realize that the object's physics parameter like mass and friction are more important in robotic manipulation. We observe that we can retrieve that information from video of real world motions. Thus, we include real-world motion in our digital asset.

A polygon mesh is defined by a set of vertices and faces, denoted as  $M = (V, F)$ , where  $V = \{\nu_1, \nu_2, \dots, \nu_n\}$  in  $\mathbb{R}^3$  represents the set of vertices and  $F = \{f_1, f_2, \dots, f_k\}$  represents the set of faces.

Similar to the 3D Gaussian Splatting [1], we use a set of 3D Gaussian kernels  $\{x_p, \sigma_p, SH_p, C_p, S_p\}_{p \in P}$ , where  $x_p$ ,  $\sigma_p$ ,  $SH_p$ ,  $C_p$ ,  $S_p$  represent the centers, opacity, covariance matrices, spherical harmonic coefficients of the Gaussians, and semantic category, respectively [49].

Consider the center of Gaussian  $A(x, y, z) \in \mathbb{R}^3$  and its corresponding image pixel location  $P(u, v) \in \mathbb{R}^2$ . We build an isomorphism such that each pixel maps to each Gaussian intersecting this pixel with the same semantic mask. Each Gaussian binds to a set of mesh vertices and faces, creating what we call Gaussian-Mesh-Pixel binding, as shown in 3.

- 1) **Projection Mapping:** Given a known camera pose represented in  $SE(3)$  and camera intrinsic, any known 3D point location can be re-projected to the 2D image plane using the perspective projection model. We denote the projection function as

$$(u, v) = \pi(x, y, z).$$

- 2) **Mesh Mapping:** An order-preserving mapping  $\mu : \mathbb{R}^3 \rightarrow V$  associates  $A$  with a vertex in  $V$ , defined as

$$\mu(x, y, z) = \{\nu_n, f_k | \nu_n \in V, f_k \in F\}.$$

- 3) **Re-projection Mapping:** Through the composition of the above mappings, we define an isomorphic relationship  $\phi$  that associates  $A$  with both  $P$  and  $V$ [5]. This

mapping is represented as

$$\phi(A) = (\pi \circ \mu)(A).$$

This mapping allows us to transfer the trajectory between the image plane recording real-world scenes, the simulation results from the mesh-based simulation engine, and the rendered 4D Gaussian Splatting Scenes [50], [51], [52], [53].

We define this binding to connect the representation of Gaussian Splatting, Mesh and Real world Motion. The gradient passing from real world video to Gaussian to mesh (backward optimization) and from mesh to Gaussian to rendered video (forward rendering) follows this binding.

#### B. Mesh extraction

We extract linkage, object, and background mesh through our mesh extraction and cleaning technique, embedding the LLM-inferred physics parameters and governing equation category(detail in Appendix) into the URDF asset based on Panoptic information. We adapt the 2DGS [30], along with a vertices cleaning and our re-orientation strategy to extract the mesh from monocular video.

The 2DGS [30] is characterized by **Center** <sub>$k$</sub> , **Tangent** =  $(t_u, t_v)$ , and **Scale** =  $(s_u, s_v)$ , which represent centers, tangential vectors, and scaling factors respectively. In 2D splatting, the normal vector is defined as  $\mathbf{N}_w = t_u \times t_v$ . A 2D Gaussian is defined in a local tangent plane in world space:

$$\mathbf{Center}(u, v) = \mathbf{center}_k + s_u \mathbf{t}_u u + s_v \mathbf{t}_v v = \mathbf{H}(u, v, 1)^T \quad (1)$$

$$\mathbf{H} = \begin{bmatrix} s_u \mathbf{t}_u & s_v \mathbf{t}_v & \mathbf{0} & \mathbf{p}_k \\ 0 & 0 & 0 & 1 \end{bmatrix} = \begin{bmatrix} \mathbf{R} \mathbf{S} & \mathbf{p}_k \\ 0 & 1 \end{bmatrix} \quad (2)$$

where  $\mathbf{H} \in \mathbb{R}^{4 \times 4}$  is a homogeneous transformation matrix representing the geometry of the 2D Gaussian. For the point  $\mathbf{u} = (u, v)$  in  $uv$  space, its 2D Gaussian value can then be evaluated by the standard Gaussian:

$$\mathcal{G}(\mathbf{u}) = \exp \left( -\frac{u^2 + v^2}{2} \right) \quad (3)$$

After obtaining the Gaussian Splatting scenes, we can extract a mesh based on its Gaussian kernel using TSDF extraction [54]. However, there are some discrepancies between the mesh generated by 2D Gaussian Splatting and the requirements for URDF production.

First, the reconstructed mesh from Gaussian Splatting does not guarantee an axis-aligned position due to the settings of Structure-from-Motion (SfM) [55]. To address this, we employ a scene re-orientation technique to align the reconstructed scenes with the simulation engine's coordinate system [16]. This alignment is crucial for replicating simulation movements and interactions in the real world with high fidelity.

The second discrepancy between the reconstructed scene and the real world is scale uncertainty, which is inevitable in scene reconstruction from monocular videos but is critical

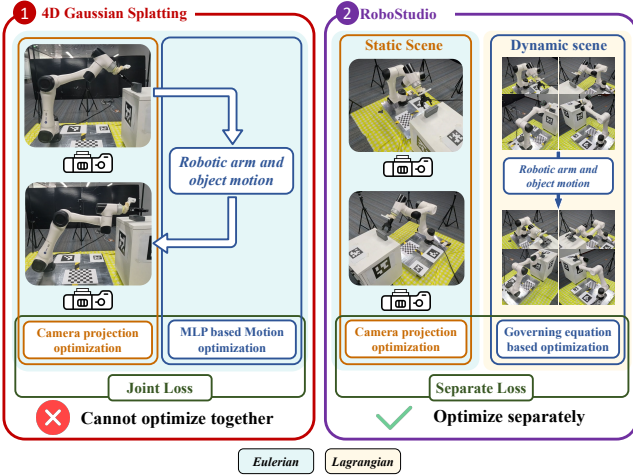


Fig. 4. Optimization of 4D Gaussian Splatting between classic MLP based method[18], [10] and Our method[51]

for robotic control and simulation. Additionally, the absolute origin is not defined in the 3D reconstruction.

Furthermore, a consistent coordinate definition is often lacking in 3D reconstructions. To address this issue, we establish a unified coordinate system that seamlessly connects real-world and simulation scenes. This unified system uses the OpenGL y-up axis, which is also employed in both Gaussian Splatting and the simulation engine.

### C. Kinematic governing equation

Optimizing 3D Gaussian Splatting involves minimizing the re-projection error between the Gaussian representation and pixel data. In 4D Gaussian Splatting, input images include both pixel data and timestamps, aiming to optimize the XYZT representation. This non-convex problem is challenging due to the lack of multi-view consistency in 4D reconstruction, as shown in 4.

We find that the optimal solution to this ill-posed problem in robotic scenes is to decompose the original 4D reconstruction problem into a two-stage process: static and dynamic stages. We treat static scenes using the Eulerian representation and dynamic scenes using the Lagrangian representation[51]. The static stage aims to optimize the camera reprojection loss, while the dynamic stage focuses on simulating the motion of objects and the robotic arm based on their corresponding governing equations. Through our mesh-pixel-Gaussian binding approach, we can pass gradients and accurately simulate the results.

In our system, control information is aligned with a predefined governing equation for physics simulation and rendering. However, when simulating these scenes in a Gaussian Splatting framework, the joint angle limits are incompatible with the discrete Gaussian setting because the spatial-temporal correspondence between joints and Gaussians cannot be accurately determined. To overcome this, we define a kinematic and dynamic system tailored for Gaussian-based robotic arm and gripper pose control.

We employ a pose-based robotic arm control strategy,

focusing on controlling the end-effector's pose and using inverse kinematics to generate control signals for each joint in the real world.

The kinematics of the robotic arm are adapted to Gaussian splatting based on modified DH parameters and coordinate changes across the Gaussian splatting, simulation, and real-world settings.

The position of a point on link  $i$  in Cartesian coordinates can be described using modified DH parameters [56]: The Denavit-Hartenberg (DH) parameters for defining the kinematics of a robotic arm include link length ( $a_i$ ), link twist ( $\alpha_i$ ), link offset ( $d_i$ ), and joint angle ( $\theta_i$ ).

The modified Denavit-Hartenberg (MDH) [56] convention uses these parameters to define the transformation matrix between consecutive coordinate frames. The transformation matrix  $T_i$  from link  $i-1$  to link  $i$  is given by:

$$T_{i-1}^i = R_x(\theta_{i-1})T_x(a_{i-1})R_z(\alpha_i)T_z(d_i)$$

$$T_i = \begin{bmatrix} \cos \theta_i & -\sin \theta_i & 0 & a_i \\ \sin \theta_i \cos \alpha_i & \cos \theta_i \cos \alpha_i & -\sin \alpha_i & -\sin \alpha_i d_i \\ \sin \theta_i \sin \alpha_i & \cos \theta_i \sin \alpha_i & \cos \alpha_i & \cos \alpha_i d_i \\ 0 & 0 & 0 & 1 \end{bmatrix}$$

The value of DH parameter can be supplied from either CAD designing, real-world measuring, or other customized values.

In this approach, the mesh serves as an interconnection mapping. The movement of each mesh is transferred through a transformation matrix to each Gaussian bound to that mesh, thereby guiding the movement of the Gaussian [57]. For example, to generate the center of a Gaussian at timestamp  $t$ ,  $P_t = (x_t, y_t, z_t)$ , we base it on its position at timestamp 0,  $P_0 = (x_0, y_0, z_0)$ .

To map points back to the base (timestamp 0):

$$\mathbf{P}_{\text{base}} = (\mathbf{T}_0^i)^{-1} \mathbf{P}_0$$

Then, to map points forward to the new frame at time  $t$ :

$$\mathbf{P}_t = \mathbf{T}_{0_t}^i \mathbf{P}_{\text{base}}$$

The overall transformation from the initial frame to the new frame at time  $t_1$ :

$$\mathbf{P}_{t_1} = \mathbf{T}_{0_t}^i (\mathbf{T}_0^i)^{-1} \mathbf{P}_0$$

Since the initial position of the robotic arm is the default position, we simply load the trajectory from the policy and transform it into the Mesh and Gaussian Splatting form.

### D. Dynamic Governing Equation

The dynamics of the rigid asset are governed by the Newton-Euler equations. The governing equation transforms the optimization problem from 6n degrees of freedom (DOF) to 6A DOF, where A is the number of movable parts defined by instance segmentation, and n is the number of Gaussian [58], [59]. This can significantly reduce the time and computational cost for the numerical solver.

Following [50] [52], we define the Newton-Euler equations as

$$\begin{bmatrix} m\mathbf{I}_{3 \times 3} & \mathbf{0} \\ \mathbf{0} & \mathbf{I} \end{bmatrix} \begin{bmatrix} \dot{\mathbf{v}} \\ \dot{\boldsymbol{\omega}} \end{bmatrix} = \begin{bmatrix} \mathbf{f} \\ \boldsymbol{\tau} \end{bmatrix} - \begin{bmatrix} \mathbf{0} \\ \boldsymbol{\omega} \times \mathbf{I}\boldsymbol{\omega} \end{bmatrix} \quad (4)$$

The simulation of forces, inertial and torque are performed in physics simulator based on our generated mesh and inferences parameter. We simply perform the semi-implicit Euler integration from Gradsim [50] for numerical solving. Dynamic governing equation will generate a transformation matrix that with force based control of robotic arm and the motion of rigid object.

The simulation of soft body can follow PAC-nerf, Phys-Gaussian and Simplicits [51], [57], [60].

### E. Rendering

The motion engine and static representation can generate accurate spatial-temporal simulations, but the rendering still needs some modification [61]. We decompose the Gaussian movement into a global transformation matrix under the supervision of kinematics and dynamics. Unlike the deformation-based 4D Gaussian Splatting [18], [62], which treats movement as an MLP deformation field, our approach explicitly updates the position of Gaussians in each timestamp and is particularly effective for objects with rigid and linked motion.

To render a view, Gaussian Splatting projects these 3D Gaussians onto the image plane. The final color of each pixel is computed as [51], [57]

$$C = \sum_{k \in P} \alpha_k S H(d_k; C_k) \prod_{j=1}^{k-1} (1 - \alpha_j). \quad (5)$$

Here,  $\alpha_k$  represents the z-depth ordered effective opacity, i.e., products of the Gaussian weights and their overall opacity  $\sigma_k$ ;  $d_k$  stands for the view direction from the camera to  $x_k$ . We only compute transformation for the  $k_{th}$  Gaussians that shares same panoptic mask with this pixel.

For the effect of global transformation matrix  $T_p^{sam}$  apply on static scenes, we decompose it into the effect of Rotation and translation:

$$f_t(d) = f_0(R^T d). \quad (6)$$

The equation  $f_t(d)$  represents the effect of rotation on the view direction of Gaussian [57].

We define  $\tau$  to represent the position update of each Gaussian center at a new time  $t$ , according to a transformation conditioned on the kinematics and dynamics of the moving part,

$$\tilde{\tau}_p(X, t, S) = R_t^S \cdot x_p^S + T_t^S. \quad (7)$$

where  $S$  indicates the instance ID of the moving part. We distill a set of trajectory from policy apply it to rendered scenes similar to [63].

## IV. EXPERIMENT

### A. Datasets:

Our datasets include various functionalities inspired by [64], [65], [66], [67]. The current dataset only contains video, language commands, and robot trajectories. Based on our implementation and research, we observe that a sufficient representation for a Real2Sim dataset should include: monocular video with panoptic labeling, bounding box information, physics parameters (details in the Appendix), mesh data, policy and trajectory information [68], [69], and real-world motion of both the object and the robotic arm under policy implementation, as well as URDF files. We find that this dataset format can encompass all the necessary information required for policy training and ensure millimeter and millisecond-level precision.

### B. Rendering:

We compare the current state-of-the-art in 4D Gaussian splatting, including SC-GS [18] and K-Planes [70], with our method. We find that both K-Planes and SC-GS fail to optimize the transformation of the robotic arm and object motion.

Figure 5 shows the reconstruction of a robotic arm performing a set of trajectories to identify its corner cases. Our method demonstrates the capability to handle complex trajectories and motions.

Figure 6 shows the reconstruction of a robotic arm pushing a box. It is evident that K-Planes and SC-GS fail to accurately reconstruct the dynamic motion of the robotic arm and rigid body, consistent with the results from Robo360 [64]. In contrast, our method successfully maintains motion and geometric consistency during robotic manipulation tasks.

### C. Mesh:

We compare our approach with 2DGS Original, Gausstudio, SUGAR, and scanned ground truth from a commercial 3D scanner. Our approach results in better mesh quality and enables contact-rich policy execution compared to SUGAR [27] and Gaustudio [15].

Figure 7 shows the quality of our mesh results compared with ground truth mesh and other methods. You can observe that our model successfully reconstructs the collision groups of different small modules of the robotic arm in URDF implementation.

Table I presents the quantitative results comparing Gausstudio, Sugar, Robostudio (v1), and Robostudio (Full). The difference between Robostudio (v1) and Robostudio (Full) is that Robostudio (Full) includes re-orientation and mesh-cleaning techniques in 2D Gaussian splatting (2dgs), which improve alignment and sampling.

### D. Manipulable Robotic Model:

In our approach, the simulation generates the movement of objects and the robotic arm, resulting in simulated trajectories for each object and robotic linkage. These trajectories are then transformed into the pre-timestamp global transformation matrix. We enable editing in the Isaac simulation

TABLE I  
MESH RECONSTRUCTION ABLATION STUDY

Method	MSE	F-score
Gaustudio	0.153	0.268
Sugar	0.159	0.375
Robostudio_v1	0.153	0.228
<b>Ours</b>	<b>0.151</b>	<b>0.721</b>

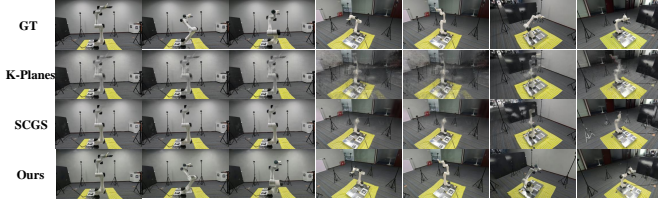


Fig. 5. Qualitative result for Novel-pose

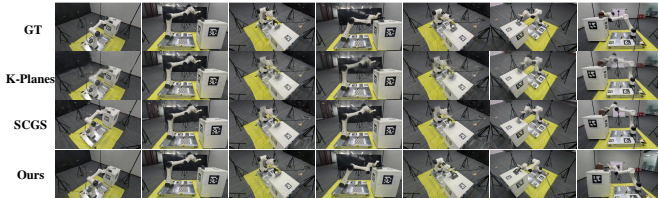


Fig. 6. Qualitative result for Push-box

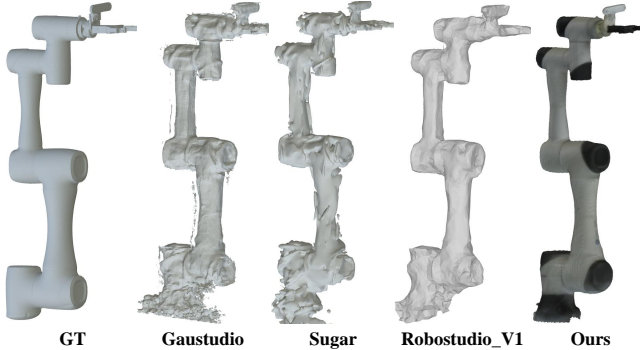


Fig. 7. Qualitative result for mesh reconstruction

backend [6] and seamless rendering in Dynamic Gaussian Splatting.

Our approach supports novel-pose and novel-policy editing. Novel-pose represents the combination of different robotic joint angles, while novel-policy allows training a position-based policy with rendering and simulation in our method. We currently support custom trajectory editing in Isaac Gym and policy implementation, demonstrating the potential for Sim2Real and Sim2Render applications based on this paradigm.

## V. CONCLUSION

Our goal was to develop a robust Real2Sim framework that significantly reduces the gap between real-world robotic manipulation tasks and their simulated counterparts. We accomplished this by introducing a hybrid representation model

that integrates mesh geometry, Gaussian color, and physics attributes. This approach ensures high-quality, realistic, and physics-consistent rendering of robotic arm manipulation scenes [24], [25]. Our model was trained and validated across various CR [8] and UR [9] product sequences, demonstrating its effectiveness in constructing accurate URDFs from video data. This method not only enhances the fidelity of simulated environments but also generalizes well to other robotic applications, thereby advancing the state-of-the-art in robotic learning and control.

Our current control approach is position-based. However, Gaussian Splatting serves as a world representation, enabling accurate rendering from any in-scene camera pose [71]. Therefore, if you want to train a vision-based policy using our assets and model, you can simply set up the render camera in our engine and use the output as training data.

## VI. APPENDIX

### Rigid Body Dynamics Variables

- $m \triangleq$  Mass of the body
- $\mathbf{I} \triangleq 3 \times 3$  inertia matrix expressed at the center of mass
- $\mathbf{f} \triangleq$  External force applied to the body
- $\boldsymbol{\tau} \triangleq$  External torque applied to the body
- $\boldsymbol{\omega} \times \mathbf{I}\boldsymbol{\omega} \triangleq$  Gyroscopic torque

### Robotic Arm Dynamics Variables

- $\theta_i \triangleq$  Angular position of joint  $i$
- $l_i \triangleq$  Length of link  $i$
- $m_i \triangleq$  Mass of link  $i$
- $I_i \triangleq$  Moment of inertia of link  $i$  about its center of mass
- $\vec{F}_i \triangleq$  External force applied to link  $i$
- $\tau_i \triangleq$  Torque applied at joint  $i$
- $\mu_i \triangleq$  Coefficient of friction at joint  $i$

### 3D Rigid Body State Representation

- $\mathbf{q}_b \triangleq [\mathbf{x}, \mathbf{r}]$ : State of a 3D rigid body, where  $\mathbf{x} \in \mathbb{R}^3$  is the position, and  $\mathbf{r} \in \mathbb{R}^4$  is a quaternion representing the orientation.
- $\mathbf{u}_b \triangleq [\mathbf{v}, \boldsymbol{\omega}]$ : Generalized velocity of the body, where  $\mathbf{v} \in \mathbb{R}^3$  is the linear velocity, and  $\boldsymbol{\omega} \in \mathbb{R}^3$  is the angular velocity.

*The predefined governing equations corresponding to each semantic category*

- **Robotic Arm:** Modified DH parameters based Kinematic model
- **Rigid Body:** Newton-Euler equations
- **Elastic Body:** Neo-Hookean elasticity

## REFERENCES

- [1] B. Kerbl, G. Kopanas, T. Leimkühler, and G. Drettakis, “3D Gaussian Splatting for Real-Time Radiance Field Rendering,” 2023.
- [2] Y. Ze, G. Yan, Y.-H. Wu, A. Macaluso, Y. Ge, J. Ye, N. Hansen, L. E. Li, and X. Wang, “GNFactor: Multi-Task Real Robot Learning with Generalizable Neural Feature Fields,” 2023.

[3] C. Li, F. Xia, R. Martín-Martín, M. Lingelbach, S. Srivastava, B. Shen, K. Vainio, C. Gokmen, G. Dharan, T. Jain, A. Kurenkov, C. K. Liu, H. Gweon, J. Wu, L. Fei-Fei, and S. Savarese, “iGibson 2.0: Object-Centric Simulation for Robot Learning of Everyday Household Tasks,” 2021.

[4] ROS, “ROS URDF,” [Online]. Available: <https://wiki.ros.org/urdf>.

[5] C. Jambon, B. Kerbl, G. Kopanas, S. Diolatzis, T. Leimkühler, and G. Drettakis, “NeRFShop: Interactive Editing of Neural Radiance Fields,” Proceedings of the ACM on Computer Graphics and Interactive Techniques, vol. 6, no. 1, 2023. [Online]. Available: <https://reposam.inria.fr/fungraph/nerfshop/>.

[6] V. Makovychuk, L. Wawrzyniak, Y. Guo, M. Lu, K. Storey, M. Macklin, D. Hoeller, N. Rudin, A. Allshire, A. Handa, and G. State, “Isaac Gym: High Performance GPU-Based Physics Simulation for Robot Learning,” 2021.

[7] C. K. Liu and D. Negruț, “The Role of Physics-Based Simulators in Robotics,” Annual Review of Control, Robotics, and Autonomous Systems, vol. 4, pp. 35–58, 2021. [Online]. Available: <https://www.annualreviews.org/content/journals/10.1146/annurev-control-072220-093055>.

[8] Sumaart.com, “CR5,” [Online]. Available: <https://www.dobot-robots.com/products/cr-series/cr5.html>.

[9] UniversalRobots, “Universal Robots,” [Online]. Available: <https://www.universal-robots.com/products/ur5-robot/>.

[10] J. Sun, H. Jiao, G. Li, Z. Zhang, L. Zhao, and W. Xing, “3DGStream: On-the-Fly Training of 3D Gaussians for Efficient Streaming of Photo-Realistic Free-Viewpoint Videos,” 2024.

[11] M. Ding, Z. Chen, T. Du, P. Luo, J. Tenenbaum, and C. Gan, “Dynamic Visual Reasoning by Learning Differentiable Physics Models from Video and Language,” Advances In Neural Information Processing Systems, vol. 34, pp. 887–899, 2021.

[12] D. Shim, S. Lee, and H. J. Kim, “SNERL: Semantic-Aware Neural Radiance Fields for Reinforcement Learning,” 2023.

[13] B. Mildenhall, P. P. Srinivasan, M. Tancik, J. T. Barron, R. Ramamoorthi, and R. Ng, “NeRF: Representing Scenes as Neural Radiance Fields for View Synthesis,” in ECCV, pp. 405–421, 2020.

[14] P. Wang, L. Liu, Y. Liu, C. Theobalt, T. Komura, and W. Wang, “NeuS: Learning Neural Implicit Surfaces by Volume Rendering for Multi-View Reconstruction,” 2023.

[15] C. Ye, Y. Nie, J. Chang, Y. Chen, Y. Zhi, and X. Han, “GauStudio: A Modular Framework for 3D Gaussian Splatting and Beyond,” 2024.

[16] M. Tancik, E. Weber, E. Ng, R. Li, B. Yi, J. Kerr, T. Wang, A. Kristoffersen, J. Austin, K. Salahi, A. Ahuja, D. McAllister, and A. Kanazawa, “NeRFStudio: A Modular Framework for Neural Radiance Field Development,” in ACM SIGGRAPH 2023 Conference Proceedings, 2023.

[17] T. Jeruzalski, D. I. W. Levin, A. Jacobson, P. Lalonde, M. Norouzi, and A. Tagliasacchi, “NiLBS: Neural Inverse Linear Blend Skinning,” 2020.

[18] Y.-H. Huang, Y.-T. Sun, Z. Yang, X. Lyu, Y.-P. Cao, and X. Qi, “SC-GS: Sparse-Controlled Gaussian Splatting for Editable Dynamic Scenes,” arXiv preprint arXiv:2312.14937, 2023.

[19] E. Šlapák, E. Pardo, M. Dopiriak, T. Maksymyuk, and J. Gazda, “Neural Radiance Fields in the Industrial and Robotics Domain: Applications, Research Opportunities and Use Cases,” 2023.

[20] T. Chen, O. Shorinwa, W. Zeng, J. Bruno, P. Dames, and M. Schwager, “Splat-Nav: Safe Real-Time Robot Navigation in Gaussian Splatting Maps,” 2024.

[21] B. P. Duisterhof, Z. Mandi, Y. Yao, J.-W. Liu, M. Z. Shou, S. Song, and J. Ichnowski, “MD-Splatting: Learning Metric Deformation from 4D Gaussians in Highly Deformable Scenes,” 2023.

[22] W. F. Whitney, T. Lopez-Guevara, T. Pfaff, Y. Rubanova, T. Kipf, K. Stachenfeld, and K. R. Allen, “Learning 3D Particle-Based Simulators from RGB-D Videos,” 2023. [Online]. Available: <https://arxiv.org/abs/2312.05359>.

[23] L. Xie, J. Julin, K. Niinuma, and L. A. Jeni, “Gaussian Splatting LK,” 2024. [Online]. Available: <https://arxiv.org/abs/2407.11309>.

[24] C. Wang, D. Gao, K. Xu, J. Geng, Y. Hu, Y. Qiu, B. Li, F. Yang, B. Moon, A. Pandey, Aryan, J. Xu, T. Wu, H. He, D. Huang, Z. Ren, S. Zhao, T. Fu, P. Reddy, X. Lin, W. Wang, J. Shi, R. Talak, K. Cao, Y. Du, H. Wang, H. Yu, S. Wang, S. Chen, A. Kashyap, R. Bandaru, K. Dantu, J. Wu, L. Xie, L. Carbone, M. Hutter, and S. Scherer, “PyPose: A Library for Robot Learning with Physics-Based Optimization,” in IEEE/CVF Conference on Computer Vision and Pattern Recognition (CVPR), 2023.

[25] Z. Zhan, X. Li, Q. Li, H. He, A. Pandey, H. Xiao, Y. Xu, X. Chen, K. Xu, K. Cao, Z. Zhao, Z. Wang, H. Xu, Z. Fang, Y. Chen, W. Wang, X. Fang, Y. Du, T. Wu, X. Lin, Y. Qiu, F. Yang, J. Shi, S. Su, Y. Lu, T. Fu, K. Dantu, J. Wu, L. Xie, M. Hutter, L. Carbone, S. Scherer, D. Huang, Y. Hu, J. Geng, and C. Wang, “PyPose v0.6: The Imperative Programming Interface for Robotics,” in IEEE/RSJ International Conference on Intelligent Robots and Systems (IROS) Workshop, 2023.

[26] M.-J. Rakotosaona, F. Manhardt, D. M. Arroyo, M. Niemeyer, A. Kundu, and F. Tombari, “NeRFMeshing: Distilling Neural Radiance Fields into Geometrically-Accurate 3D Meshes,” 2023.

[27] A. Guédon and V. Lepetit, “SUGAR: Surface-Aligned Gaussian Splatting for Efficient 3D Mesh Reconstruction and High-Quality Mesh Rendering,” 2023.

[28] I. Liu, H. Su, and X. Wang, “Dynamic Gaussians Mesh: Consistent Mesh Reconstruction from Monocular Videos,” 2024.

[29] Y. Weng, B. Wen, J. Tremblay, V. Blukis, D. Fox, L. Guibas, and S. Birchfield, “Neural Implicit Representation for Building Digital Twins of Unknown Articulated Objects,” in CVPR, 2024.

[30] B. Huang, Z. Yu, A. Chen, A. Geiger, and S. Gao, “2D Gaussian Splatting for Geometrically Accurate Radiance Fields,” in SIGGRAPH 2024 Conference Papers, 2024.

[31] Z. Wu, T. Liu, L. Luo, Z. Zhong, J. Chen, H. Xiao, C. Hou, H. Lou, Y. Chen, R. Yang, et al., “MARS: An Instance-Aware, Modular and Realistic Simulator for Autonomous Driving,” in CAAI International Conference on Artificial Intelligence, Springer, 2023, pp. 3–15.

[32] Q. Dai, Y. Zhu, Y. Geng, C. Ruan, J. Zhang, and H. Wang, “Grasp-NeRF: Multiview-Based 6-DOF Grasp Detection for Transparent and Specular Objects Using Generalizable NeRF,” 2023. [Online]. Available: <https://arxiv.org/abs/2210.06575>.

[33] I. Kapelyukh, V. Vosylius, and E. Johns, “DALL-E-Bot: Introducing Web-Scale Diffusion Models to Robotics,” IEEE Robotics and Automation Letters, vol. 8, no. 7, pp. 3956–3963, 2023. [Online]. Available: <https://dx.doi.org/10.1109/LRA.2023.3272516>.

[34] F. Zhu, H. Wu, S. Guo, Y. Liu, C. Cheang, and T. Kong, “IRASim: Learning Interactive Real-Robot Action Simulators,” arXiv preprint arXiv:2406.12802, 2024.

[35] Y. Jiang, C. Wang, R. Zhang, J. Wu, and L. Fei-Fei, “TransIC: Sim-to-Real Policy Transfer by Learning from Online Correction,” 2024. [Online]. Available: <https://arxiv.org/abs/2405.10315>.

[36] G. Lu, S. Zhang, Z. Wang, C. Liu, J. Lu, and Y. Tang, “ManiGaussian: Dynamic Gaussian Splatting for Multi-Task Robotic Manipulation,” 2024.

[37] K. Wang, W. R. J. III, S. Lu, X. Huang, J. Booth, R. Kramer-Bottiglio, M. Aanjaneya, and K. Bekris, “Real2Sim2Real Transfer for Control of Cable-Driven Robots via a Differentiable Physics Engine,” [Online]. Available: <https://par.nsf.gov/biblio/10493921>.

[38] V. Lim, H. Huang, L. Y. Chen, J. Wang, J. Ichnowski, D. Seita, M. Laskey, and K. Goldberg, “Real2Sim2Real: Self-Supervised Learning of Physical Single-Step Dynamic Actions for Planar Robot Casting,” in 2022 International Conference on Robotics and Automation (ICRA), 2022, pp. 8282–8289.

[39] J. Whitman and H. Choset, “Learning Modular Robot Visual-Motor Locomotion Policies,” 2023. [Online]. Available: <https://arxiv.org/abs/2210.17486>.

[40] K. Ehsani, T. Gupta, R. Hendrix, J. Salvador, L. Wehs, K.-H. Zeng, K. P. Singh, Y. Kim, W. Han, A. Herrasti, R. Krishna, D. Schwenk, E. VanderBilt, and A. Kembhavi, “Imitating Shortest Paths in Simulation Enables Effective Navigation and Manipulation in the Real World,” 2023. [Online]. Available: <https://arxiv.org/abs/2312.02976>.

[41] D. Coleman, I. Sucan, S. Chitta, and N. Correll, “Reducing the Barrier to Entry of Complex Robotic Software: A MoveIt! Case Study,” 2014.

[42] Y.-L. Qiao, J. Liang, V. Koltun, and M. C. Lin, “Efficient Differentiable Simulation of Articulated Bodies,” in Proceedings of the 38th International Conference on Machine Learning, vol. 139, 2021, pp. 8661–8671. [Online]. Available: <https://proceedings.mlr.press/v139/qiao21a.html>.

[43] Y. Zheng, X. Chen, Y. Zheng, S. Gu, R. Yang, B. Jin, P. Li, C. Zhong, Z. Wang, L. Liu, C. Yang, D. Wang, Z. Chen, X. Long, and M. Wang, “GaussianGrasper: 3D Language Gaussian Splatting for Open-Vocabulary Robotic Grasping,” 2024.

[44] B. Chen, R. Kwiatkowski, C. Vondrick, and H. Lipson, “Full-Body Visual Self-Modeling of Robot Morphologies,” 2021.

[45] Z. Zhong, J. Cao, S. Gu, S. Xie, W. Gao, L. Luo, Z. Yan, H. Zhao, and

G. Zhou, "ASSIST: Interactive Scene Nodes for Scalable and Realistic Indoor Simulation," 2023.

[46] M. Bauza, A. Bronars, Y. Hou, I. Taylor, N. Chavan-Dafle, and A. Rodriguez, "SIMPLE, a Visuotactile Method Learned in Simulation to Precisely Pick, Localize, Regrasp, and Place Objects," *Science Robotics*, vol. 9, no. 91, eadi8808, 2024. [Online]. Available: <https://www.science.org/doi/abs/10.1126/scirobotics.adi8808>.

[47] H. Ha, Y. Gao, Z. Fu, J. Tan, and S. Song, "UMI on Legs: Making Manipulation Policies Mobile with Manipulation-Centric Whole-Body Controllers," 2024. [Online]. Available: <https://arxiv.org/abs/2407.10353>.

[48] A. Chakra Jad, K. Rana, F. Dayoub, and N. Sünderhauf, "Physically Embodied Gaussian Splatting: Embedding Physical Priors into a Visual 3D World Model for Robotics," [Online]. Available: <https://embodied-gaussians.github.io/>.

[49] A. Author, "LiveScene: Language Embedding Interactive Radiance Fields for Physical Scene Rendering and Control," 2024.

[50] K. M. Jatavallabhula, M. Macklin, F. Golemo, V. Voleti, L. Petrini, M. Weiss, B. Considine, J. Parent-Levesque, K. Xie, K. Erleben, L. Paull, F. Shkurti, D. Nowrouzezahrai, and S. Fidler, "GradSim: Differentiable Simulation for System Identification and Visuo-Motor Control," in *International Conference on Learning Representations (ICLR)*, 2021.

[51] X. Li, Y.-L. Qiao, P. Y. Chen, K. M. Jatavallabhula, M. Lin, C. Jiang, and C. Gan, "PAC-NeRF: Physics Augmented Continuum Neural Radiance Fields for Geometry-Agnostic System Identification," 2023.

[52] E. Sifakis and J. Barbic, "FEM Simulation of 3D Deformable Solids: A Practitioner's Guide to Theory, Discretization and Model Reduction," in *ACM SIGGRAPH 2012 Courses*, 2012. [Online]. Available: <https://doi.org/10.1145/2343483.2343501>.

[53] Y. Jiang, C. Yu, T. Xie, X. Li, Y. Feng, H. Wang, M. Li, H. Lau, F. Gao, Y. Yang, and C. Jiang, "VR-GS: A Physical Dynamics-Aware Interactive Gaussian Splatting System in Virtual Reality," *arXiv preprint arXiv:2401.16663*, 2024.

[54] J. Choe, S. Im, F. Rameau, M. Kang, and I. S. Kweon, "VolumeFusion: Deep Depth Fusion for 3D Scene Reconstruction," 2021. [Online]. Available: <https://arxiv.org/abs/2108.08623>.

[55] L. Pan, D. Baráth, M. Pollefeys, and J. L. Schönberger, "Global Structure-from-Motion Revisited," 2024. [Online]. Available: <https://arxiv.org/abs/2407.20219>.

[56] P. I. Corke, "A Simple and Systematic Approach to Assigning Denavit–Hartenberg Parameters," *IEEE Transactions on Robotics*, vol. 23, no. 3, pp. 590–594, 2007.

[57] T. Xie, Z. Zong, Y. Qiu, X. Li, Y. Feng, Y. Yang, and C. Jiang, "Phys-Gaussian: Physics-Integrated 3D Gaussians for Generative Dynamics," *arXiv preprint arXiv:2311.12198*, 2023.

[58] R.-Z. Qiu, G. Yang, W. Zeng, and X. Wang, "Feature Splatting: Language-Driven Physics-Based Scene Synthesis and Editing," 2024.

[59] C. M. Kim, M. Wu, J. Kerr, M. Tancik, K. Goldberg, and A. Kanazawa, "Garfield: Group Anything with Radiance Fields," in *arXiv*, 2024.

[60] V. Modi, N. Sharp, O. Perel, S. Sueda, and D. I. Levin, "Simplicits: Mesh-Free, Geometry-Agnostic, Elastic Simulation," *arXiv preprint*, 2024.

[61] Y. Li, J. Wu, R. Tedrake, J. B. Tenenbaum, and A. Torralba, "Learning Particle Dynamics for Manipulating Rigid Bodies, Deformable Objects, and Fluids," 2019.

[62] Z. Yang, X. Gao, W. Zhou, S. Jiao, Y. Zhang, and X. Jin, "Deformable 3D Gaussians for High-Fidelity Monocular Dynamic Scene Reconstruction," *arXiv preprint arXiv:2309.13101*, 2023.

[63] M. Torne, A. Simeonov, Z. Li, A. Chan, T. Chen, A. Gupta, and P. Agrawal, "Reconciling Reality Through Simulation: A Real-to-Sim-to-Real Approach for Robust Manipulation," 2024.

[64] L. Liang, L. Bian, C. Xiao, J. Zhang, L. Chen, I. Liu, F. Xiang, Z. Huang, and H. Su, "Robo360: A 3D Omnispective Multi-Material Robotic Manipulation Dataset," 2023.

[65] Z. Fu, T. Z. Zhao, and C. Finn, "Mobile ALOHA: Learning Bimanual Mobile Manipulation with Low-Cost Whole-Body Teleoperation," in *arXiv*, 2024.

[66] O. X.-E. Collaboration, A. O'Neill, A. Rehman, et al., "Open X-Embodiment: Robotic Learning Datasets and RT-X Models," 2023. [Online]. Available: <https://arxiv.org/abs/2310.08864>.

[67] H. Liu, C. Ye, Y. Nie, Y. He, and X. Han, "LASA: Instance Reconstruction from Real Scans Using a Large-Scale Aligned Shape Annotation Dataset," *arXiv preprint arXiv:2312.12418*, 2023.

[68] Q. Wang, Y.-Y. Chang, R. Cai, Z. Li, B. Hariharan, A. Holynski, and N. Snavely, "Tracking Everything Everywhere All at Once," *ICCV*, 2023.

[69] Y. Xiao, Q. Wang, S. Zhang, N. Xue, S. Peng, Y. Shen, and X. Zhou, "SpatialTracker: Tracking Any 2D Pixels in 3D Space," 2024.

[70] S. Fridovich-Keil, G. Meanti, F. Warburg, B. Recht, and A. Kanazawa, "K-Planes: Explicit Radiance Fields in Space, Time, and Appearance," 2023.

[71] S. B. Bowen, W. Wei, Y. Yang, and J. Kautz, "FoundationPose: Unified 6D Pose Estimation and Tracking of Novel Objects," in *CVPR*, 2024.